Linear Correlation between Active and Resistive Stresses Provides Information on Force Generation and Stress Transmission in Adherent Cells

Hélène Delanoë-Ayari,[1,*] Nicolas Bouchonville,[2] Marie Courçon,[3] and Alice Nicolas[2,†]
[1]Université de Lyon, Université Claude Bernard Lyon 1, CNRS, Institut Lumière Matière, F-69622, Villeurbanne, France
[2]Université Grenoble Alpes, CNRS, LTM, 38000 Grenoble, France
[3]Université Grenoble Alpes, CEA, Inserm, BIG-BGE, 38000 Grenoble, France

(Received 19 May 2021; accepted 18 May 2022; published 24 August 2022)

Animal cells are active, contractile objects. While bioassays address the molecular characterization of cell contractility, the mechanical characterization of the active forces in cells remains challenging. Here by confronting theoretical analysis and experiments, we calculated both the resistive and the active components of the intracellular stresses that build up following cell adhesion. We obtained a linear relationship between the divergence of the passive stress and the traction forces, which we show is the consequence of the cell adhering and applying forces on the surface only through very localized adhesion points (whose size is inferior to our best resolution, of 400 nm). This entails that there are no measurable forces outside of these active point sources, and also that the passive stresses and active stresses inside cells are proportional.

DOI: 10.1103/PhysRevLett.129.098101

Animal cells have contractile capabilities that make cells tensed objects. This contractility allows adherent cells to probe the mechanical properties of their environment and adapt to them [1–3]. Dysfunction of cell contractility is a hallmark of many pathologies, such as cancers, cardiac, or brain pathologies [4,5]. As it is strictly regulated and adapts to external physical or chemical perturbations [6], the analysis of cell contractility often brings information on the interplay of specific signaling pathways with the extracellular environment. For example, stem cell differentiation was shown to be closely regulated by the level of contractility of the tissue they are part of [7]. When asking about cell contractility, the biological question is in general to identify, locate, and quantify the biochemical processes in cells that give rise to cellular forces, contractile or tensile stresses. The activity of molecular motors, for instance, results in mechanical stresses [2,8]. Changes in the conformation of these proteins generate molecular movements that mechanically translate into generation of forces at the molecular level. In cell biology, these sources of stress are sought using molecular markers thus setting assumptions on the biological nature of the intracellular stress generators.

More recently, a need for label-free approaches to assess cell contractility has emerged. Their objective is to identify the areas of stress generation and to quantify their amplitude. Optical methods have been proposed that measure the density of cytoskeleton fibers in the absence of staining [9]. With even less assumption on the origin of stress generation, mechanical approaches have been implemented that quantify intracellular mechanical stresses [10–13]. These methods are based on the measurement of the deformation of the extracellular environment the cells are adhering to and exploit it to calculate cell internal stresses. Here we focus on these mechanical approaches.

By combining them as described in Ref. [14], we observe a linear correlation between the active and resistive components of the intracellular stress tensors. Complementing this observation with theoretical approaches, we bring a new picture of the interaction of the cells with the substrate, showing the existence of discrete mechanical links between the stress generators and the substrate at submicron scale.

There exist different techniques for calculating cellular stress in cells. One set of methods is based on the writing of force conservation inside a 2D material. It uses as input the traction forces exerted by the cells on its environment and solves the 2D equation

$$h div(S_{\mathrm{tot}}) = \vec{f}_m, \tag{1}$$

where $\vec{f}_m$ is the surface force field exerted by the substrate on the cells and h the mean height of the cell, see Fig. 1. One can either solve this equation using standard finite element in the way proposed by Tambe *et al.* [15] for monolayer stress microscopy (MSM) or use a Bayesian approach as proposed by Nier *et al.* [13] for Bayesian inference stress microscopy (BISM). Both these techniques enable to recover the total stress inside the monolayer, $S_{\mathrm{tot}} = S_{\mathrm{act}} + S_c$, which is the sum of the active and passive resistive stress in the cell arising from

$$\vec{f}_{\mathrm{act}} + \vec{f}_c - \vec{f}_m = \vec{0}, \tag{2}$$

 © 2022 American Physical Society

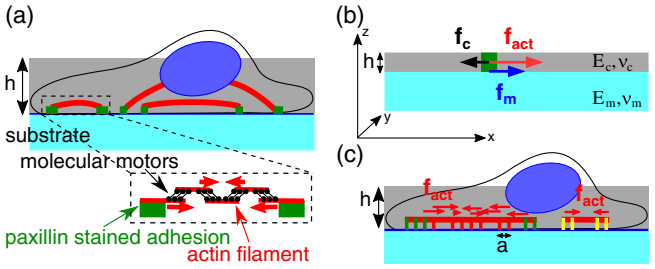

FIG. 1. Modeling of an adherent cell for intracellular stress calculation. (a) Schematic of an adherent cell. Acto-myosin filaments (in red) are attached to focal adhesions (in green) and may raise tension in cell body. h is the thickness of the layer where the stresses transmitted to the substrate are generated. (b) Elastic model for a cell or a cell colony (in gray) firmly adhered to a semi-infinite deformable matrix (in blue). The respective Young's moduli for the thin film and the semi-infinite layer are E_c and E_m and their Poisson's ratio ν_c and ν_m. The cell is assumed to bear a point of stress generation, $\vec{f}_{\mathrm{act}}$ (red square). The thin film opposes a resistance $\vec{f}_c$ to the active stress, and the matrix opposes $-\vec{f}_m$. (c) Our results indicate that intracellular stresses are transmitted to the substrate through discrete anchorages of size smaller than the experimental sampling size a. This transmission could either come from discrete connections of the stress generators (e.g., the acto-myosin stress fibers and paxillin-stained adhesions) or of unstained adhesion sites (depicted in yellow).

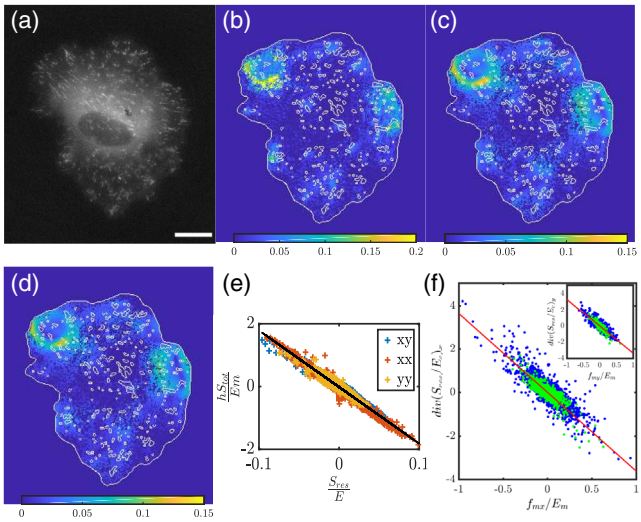

FIG. 2. (a) Focal adhesions in REF52 stably transfected for YFP-paxillin. Bar 20 μm. (b) Amplitude of $\vec{f}_m/E_m$ superimposed with the cell contour and the contour of the paxillin-stained adhesions (in white) shows significant stresses out of paxillin-stained adhesions. (c) Amplitude of S_c/E_c measured at places where $\vec{f}_m$ exceeds noise level. (d) Amplitude of hS_{tot}/E_m in μm, calculated at the same places (regularization parameter $L = 0.06$). (e) The components of hS_{tot}/E_m and S_c/E_c show a linear correlation (slope 2.28 $\mu\mathrm{m}^{-1}$). (f) The components of $divS_c/E_c$ and $\vec{f}_m/E_m$ are proportional (slope 2.27 $\mu\mathrm{m}^{-1}$). Green dots are for paxillin-labeled pixels, blue dots for unlabeled pixels.

with $\vec{f}_{\mathrm{act}}$ the active cellular forces that cells build up following adhesion and $\vec{f}_c$ the reaction force of the cell body. On the contrary, as shown in Ref. [14], intracellular stress microscopy (ISM) enables to recover the Young's modulus-normalized resistive stress tensor S_c/E_c. This latter technique does not require the calculation of the forces from the cells to the substrate, but is based solely on the continuity of the displacement at the interface of the cell and the substrate interface [12]. For cell biology issues, a quantity of prime interest is $\vec{f}_{\mathrm{act}}$, the internal cellular surface forces at the origin of cell contractility. In principle, combination of MSM or BISM and ISM will provide hS_{act} from which $\vec{f}_{\mathrm{act}}$ can be derived. We thus decided to calculate both quantities S_{tot} and S_c using BISM and ISM, and we present here an in-depth exploration of their relationship obtained in two different cell types.

We first investigated the intracellular stresses in rat embryonic fibroblast cell line REF52 (Fig. 2). The REF52 cell line we used was stably transfected with fluorescent paxillin (gift from A. Bershadsky), so to compare the location of intracellular stresses and paxillin stained focal adhesions. The geometry of the single cells was consistent with the plaque approximation, the height of the cells being at a maximum of 5 μm (data not shown) to be compared to their in-plane extent of order of 50 to 100 μm. Single cells were grown on a soft polyacrylamide hydrogel of 3 kPa functionalized with fibronectin. The hydrogel was loaded with a high density of 200 nm fluorescent markers. The deformation field of the substrate was quantified by comparing images of beads located close to its top surface in the presence of cells and when the cells are removed. Beads displacements were measured using a pyramidal optical flow algorithm [16]. The surface forces $\vec{f}_m$ were calculated using fast Fourier transformation of the displacement field [24]. We first observed that the traction force field did not evidence correlations with the distribution of the paxillin-stained adhesions [Fig. 2(b)]. This suggests that cell intracellular stresses are transmitted to the extracellular matrix also out of these adhesions. This result is not surprising as Zamir *et al.* have shown that in REF 52 cells paxillin staining does not stain tensin rich focal adhesions [25]. This again promotes a label-free approach, as one can never be sure that labeling one (or even several proteins) will guarantee the observation of all sites of interest for active stress generation.

Since the calculation of S_c by ISM only makes sense when the cell body is firmly bound to the substrate, we limited stress calculation to paxillin-positive regions and to regions where $\vec{f}_m$ is above the noise level [Fig. 2(c)]. In these regions, the fact that the traction force field $\vec{f}_m$ is out of the noise implies that the cell is adhered and intracellular stresses are transmitted to the substrate. S_{tot} was calculated in the same regions using BISM algorithm, following the methodology described in Ref. [14] [Fig. 2(d)]. Comparison of

BISM and ISM revealed a linear correlation between both, with a negative slope [Fig. 2(e)]. In addition, following a previous work where we had reported on a linear relationship between the amplitudes of $divS_c$ and $\vec{f}_m$ [12], we confirmed this linear correlation for this other cell type. Components of the divergence of the resistive stress tensor S_c correlate with surface force components $\vec{f}_m$ with a minus sign [Fig. 2(f)]:

$$div\frac{S_c}{E_c} = -\frac{\vec{f}_m}{\ell E_m}, \tag{3}$$

with E_m the Young's modulus of the matrix and ℓ a characteristic length. As visible on Fig. 2(f), positively paxillin-labeled pixels are indistinguishable from unlabeled pixels. This observation provides an additional argument for enlarging the regions of cell adhesion out of paxillin-positive adhesions [12].

To understand these linear correlations, we calculated the theoretical relationship between $divS_c$ and $\vec{f}_m$ in a model system that consists of a thin elastic layer continuously bound to a semi-infinite elastic medium and stressed by a local stress field [see Fig. 1(b)]. As the surface forces $\vec{f}_m$ are linked to the displacement field through Green's function [26], the relationship between $divS_c$ and $\vec{f}_m$ is of similar shape: a nonlocal relationship, with a combined influence of the stresses from both in-plane directions. We, however, obtained that this nonlocal relationship can be approximated to a local proportionality because (i) the off-diagonal terms in the Green's function are 2 orders of magnitude smaller than the diagonal terms, and (ii) the diagonal terms are fast decaying functions close to the force point (Supplemental Material SI-2 [16]). Because of this fast decay, the relationship between $divS_c$ and $\vec{f}_m$ is sensitive to the ratio of the lateral extent of $\vec{f}_m$ and the sampling size of the grid that is used to perform traction force microscopy (TFM) or stress calculations. Actually, a linear correlation between $divS_c$ and $\vec{f}_m$ was obtained when the lateral extent of the surface forces $\vec{f}_m$ is smaller than the sampling size [Figs. 3 and S3(a)–S3(c) in Ref. [16]]. The opposite case, where the amplitude of the surface forces spreads on a width larger than the sampling size leads to a nonlinear correlation, different from the experimental observation [Figs. 3 and S3(d)–S3(f) [16]]. Facing the model with the experimental observation thus leads to the conclusion that the traction forces $\vec{f}_m$ apply on areas that are smaller than the size of the sampling grid that is used in TFM. So due to the size of the sampling, $\vec{f}_m$ appears as point forces. The model then predicts

$$hdivS_c = \vec{f}_c \simeq -\alpha\vec{f}_m, \tag{4}$$

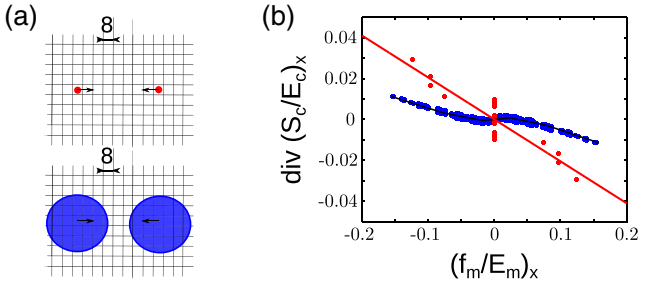

FIG. 3. Analysis of the correlation of $divS_c$ and $\vec{f}_m$. (a) Scheme of the protocol used for calculating curves drawn in (b). A dipole force with a Gaussian distribution whose width σ is either smaller (larger) than the sampling size a (top, bottom) is simulated for calculating the divergence of Sc according to Eq. (S8). (b) $divS_c$ and $\vec{f}_m$ show a linear correlation when $\sigma < a$ ($a = 8$ pixels, red: $\sigma = 1$ pixel; blue: $\sigma = 25$ pixels). Goodness of the fit for the red curve: $r^2 = 0.83$. The dark line is a bin average of the blue points.

where $\alpha = [\pi h E_c(1+\nu_m)(3-2\nu_m-\nu_c)/3aE_m(1-\nu_c^2)]$ with a the size of the sampling grid and ν_c and ν_m the Poisson's ratios of the cell and the substrate. The direct calculation of the Green's function (SI-2 [16]) confirmed a close to linear relationship between $divS_c$ and $\vec{f}_m$ for $\vec{f}_m$ profiles narrower than the sampling size (Fig. 3). For wider distributions of $\vec{f}_m$, the correlation showed two branches [Fig. 3(b)], also observed in 3D FEM simulation [14], a consequence of the oscillations of the Green's function that couples both quantities (Fig. S2 [16]). From this analysis, we could conclude that the proportionality between $divS_c$ and $\vec{f}_m$ that we observe in the experiment is indeed related to the small extent of the traction forces compared to the sampling size, and is anyhow an approximate linearity. Combined with the observation that the amplitude of $\vec{f}_m$ is above the noise level in a large part of the cell (Fig. S6 [16]), we conclude that the surface forces $\vec{f}_m$ are concentrated to very local areas whose size is below our in-plane resolution of 0.7 μm, but are distributed almost everywhere beneath the cell, not restricted to paxillin-stained adhesions.

Equation (3) has introduced a characteristic length scale ℓ that should compare to $1/\alpha$ in Eq. (4). We artificially reduced the in-plane resolution to probe the dependency of ℓ with the sampling size a. As shown in Fig. S4 of the Supplemental Material [16], we obtained that ℓ is proportional to a, as predicted in Eq. (4) (see SI-3 [16]). This confirmed our analysis on the role of the sampling size in the relation between $divS_c$ and $\vec{f}_m$. Combination of Eqs. (2) and (4) then implies that at points where $\vec{f}_m \neq \vec{0}$,

$$\vec{f}_{\mathrm{act}} \simeq (1+\alpha)\vec{f}_m \tag{5}$$

and Eqs. (1) and (4) lead to

$$S_c \simeq -\alpha S_{\mathrm{tot}} + \Phi. \tag{6}$$

This second linear correlation is a direct consequence of the linear correlation between $divS_c$ and $\vec{f}_m$. It should be noted that linearity is optimal when the regularization parameter in the BISM calculation is chosen with the χ^2 principle (see SI-1 and Fig. S7 [16]).

We wondered whether the linear correlation between $\vec{f}_m$ and $divS_c$ we observed with REF 52 cells was specific to the experimental conditions used here. To test the robustness of our observations, Fritzsch's group made available raw data obtained with Hela cells expressing GFP-paxillin cultured on a 40 kPa polyacrylamide hydrogel loaded with fluorescent beads of 40 nm diameter [27] (Fig. 4). The position of the beads was imaged with STED microscopy, as described in Ref. [28]. In this experiment, the pixel size is about 20 nm to be compared to 100 nm in our experiment. The much stiffer substrate allowed cells to develop more mature focal adhesions, although it may limit our capability to detect small stresses as small deformations may be hidden by the noise. The enhanced resolution of STED microscopy allowed us to reach a spatial resolution of 400 nm, 2000 beads being successfully tracked in the image. Figure 4(b) shows the calculated displacement field of the beads. Here, large traction forces were observed in focal adhesions at the periphery of the cell [Fig. 4(c)]. For the first time, thanks to the enhanced resolution, alternating compressive and tensile stresses were made visible within the focal adhesions [Fig. 4(d)], as predicted by theories that address the growth of focal adhesions in the force direction [29,30]. We retrieve here, without any labeling, one of the results obtained with molecular stress tensors, i.e., local heterogenities of stresses under adhesive patches [31]. As for the REF 52 cells grown on a much softer substrate, a linear correlation between $divS_c/Ec$ and $\vec{f}_m/E_m$ was observed [Fig. 4(e)]. This confirms that this relation does not come from bias in the experimental setup. So we conclude that the measurement of the traction forces $\vec{f}_m$ gives information on the location of the intracellular stress generators [Fig. 1(d)].

In conclusion, we report on a linear correlation between the divergence of the stress tensor in the cell body and the forces that are transmitted to the substrate [Fig. 2(f)]. This linear relation implies that independent of any assumption on the rheological properties of the cell body, the transmission of the cellular stresses to the substrate is performed through local links whose size is smaller than the sampling size of the experiment, as depicted in Fig. 1(d). When the cells have a linear elastic behavior, we show that stress generation following cell adhesion leads as a first approximation to the production of a proportional resistive stress in the cell body. Thus, quantification of the intracellular stresses either by MSM, BISM, or ISM brings similar qualitative results. It also makes it possible to localize stress generators by measuring the surface forces $\vec{f}_m$ that cells transmit to the extracellular environment thus highlighting the sensitivity and the relevance of mechanical analysis as companion technique of biological analysis.

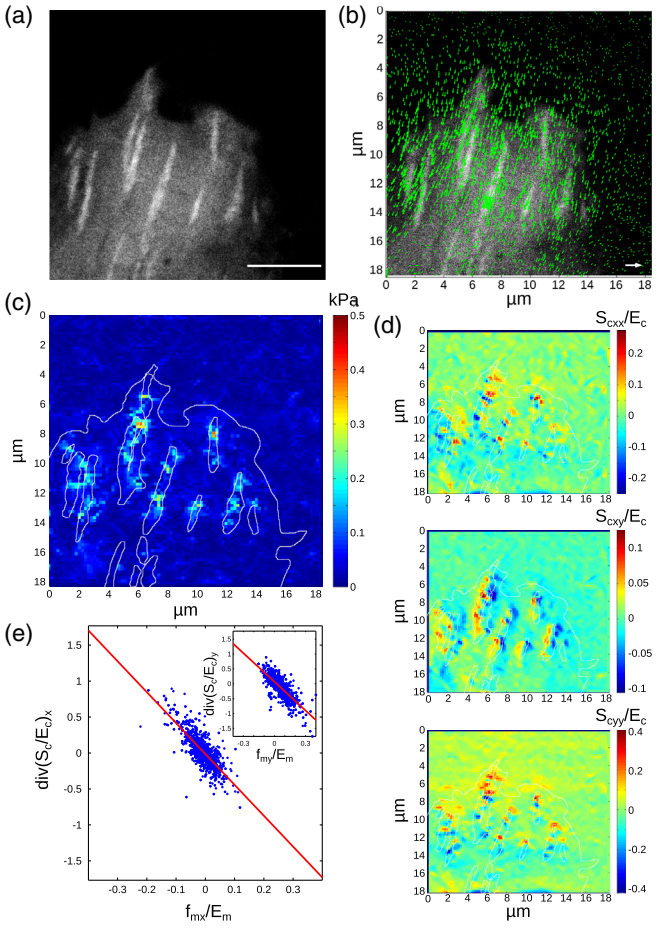

FIG. 4. (a) Paxillin expressing Hela cells on 40 kPa polyacrylamide hydrogels imaged with STED microscopy. Bar 5 μm. (b) Displacement field obtained with the KLT optical flow algorithm. The white arrow is 0.5 μm long. (c) Traction forces concentrate in focal adhesions and show dotted patterns. White lines delineate cell periphery and focal adhesions. (d) Maps of the stress components, superimposed with the contours of the cell and the focal adhesions (white lines). Local compressive and tensile stresses are visible within focal adhesions. (e) The linear correlation between $\vec{f}_m/E_m$ and $div(S_c/E_c)$ is still observed with these mature focal adhesions. Raw data were kindly provided by H. Colin-York and M. Fritzsche on our demand.

The authors are indebted to D. Gulino-Debrac for allowing them to use the biology lab and to P. Marcq for the provision of the BISM calculation code. A. N. and H. D.-A. deeply acknowledge H. Colin-York and M. Fritzsche for providing additional raw data to test the accuracy of the analysis. This work was initiated by very

fruitful discussions with E. Mazza, L. Filotto, P. Silberzan, and T. Vourc'h. H. D. and A. N. are grateful to them. The authors also thank F. Graner for critical reading. A. N. and N. B. acknowledge the support by ANR-12-JSVE05-0008.

*helene.delanoe-ayari@univ-lyon1.fr
†alice.nicolas@cea.fr

[1] T. R. Polte, G. S. Eichler, N. Wang, and D. E. Ingber, Am. J. Physiol. Cell Physiol. **286**, C518 (2004).
[2] B. L. Doss, M. Pan, M. Gupta, G. Grenci, R.-M. Mège, C. T. Lim, M. P. Sheetz, R. Voituriez, and B. Ladoux, Proc. Natl. Acad. Sci. U.S.A. **117**, 12817 (2020).
[3] J. Zhang, F. Alisafaei, M. Nikolić, X. A. Nou, H. Kim, V. B. Shenoy, and G. Scarcelli, Small **16**, 1907688 (2020).
[4] J. M. Northcott, I. S. Dean, J. K. Mouw, and V. M. Weaver, Front. Cell Dev. Biol. **6**, 17 (2018).
[5] M. Javier-Torrent and C. A. Saura, Cells **9**, 1926 (2020).
[6] F. Bordeleau and C. A. Reinhart-King, F1000Research **5**, 1819 (2016).
[7] W. Ning, A. Muroyama, H. Li, and T. Lechler, Cell Stem Cell **28**, 436 (2021).
[8] S. R. Peyton, C. M. Ghajar, C. B. Khatiwala, and A. J. Putnam, Cell Biochem. Biophys. **47**, 300 (2007).
[9] W. Wang, J. P. Miller, S. C. Pannullo, C. A. Reinhart-King, and F. Bordeleau, J. Biophoton. **11**, e201800008 (2018).
[10] N. Wang, I. M. Tolić-Nørrelykke, J. Chen, S. M. Mijailovich, J. P. Butler, J. J. Fredberg, and D. Stamenović, Am. J. Physiol. Cell Physiol. **282**, C606 (2002).
[11] D. T. Tambe, C. Corey Hardin, T. E. Angelini, K. Rajendran, C. Y. Park, X. Serra-Picamal, E. H. Zhou, M. H. Zaman, J. P. Butler, D. A. Weitz, J. J. Fredberg, and X. Trepat, Nat. Mater. **10**, 469 (2011).
[12] M. Moussus, C. der Loughian, D. Fuard, M. Courçon, D. Gulino-Debrac, H. Delanoë-Ayari, and A. Nicolas, Soft Matter **10**, 2414 (2014).
[13] V. Nier, S. Jain, C. T. Lim, S. Ishihara, B. Ladoux, and P. Marcq, Biophys. J. **110**, 1625 (2016).
[14] H. Delanoë-Ayari and A. Nicolas, companion paper, Phys. Rev. E **106**, 024411 (2022).
[15] D. T. Tambe, U. Croutelle, X. Trepat, C. Y. Park, J. H. Kim, E. Millet, J. P. Butler, and J. J. Fredberg, PLoS One **8**, e55172 (2013).
[16] See Supplemental Material at http://link.aps.org/supplemental/10.1103/PhysRevLett.129.098101 for Material and Methods, analytical analysis, effects of sampling and filtering, influence of cell rheology on final results and supplementary figures, which includes Refs. [17–23].
[17] A. Barbacci, J. Diener, P. Hémon, B. Adam, N. Donès, L. Reveret, and B. Moulia, Agr. Forest Meteorol. **184**, 220 (2014).
[18] B. D. Lucas and T. Kanade, in *International Joint Conference on Artificial Intelligence* (1981), pp. 674–679.
[19] C. N. Holenstein, U. Silvan, and J. G. Snedeker, Sci. Rep. **7**, 41633 (2017).
[20] J. Y. Bouguet, Pyramidal implementation of the Lucas Kanade feature tracker description of the algorithm, Intel Corporation, Microprocessor Research Labs, OpenCV Documentation, 2001.
[21] Z. I. Kalcioglu, R. Mahmoodian, Y. Hu, Z. Suo, and K. J. Van Vliet, Soft Matter **8**, 3393 (2012).
[22] B. Sabass, M. L. Gardel, C. M. Waterman, and U. S. Schwarz, Biophys. J. **94**, 207 (2008).
[23] N. Nijenhuis, X. Zhao, A. Carisey, C. Ballestrem, and B. Derby, Biophys. J. **107**, 1502 (2014).
[24] J. P. Butler, I. Tolić-Nørrelykke, B. Fabry, and J. J. Fredberg, Am. J. Physiol. Cell Physiol. **282**, C595 (2002).
[25] E. Zamir, B. Z. Katz, S.-i. Aota, K. M. Yamada, B. Geiger, and Z. Kam, J. Cell Sci. **112**, 1655 (1999).
[26] L. D. Landau and E. M. Lifshitz, *Theory of Elasticity*, 2nd ed., Course of Theoretical Physics Vol. 7 (Pergamon Press, Oxford, 1970).
[27] H. Colin-York, C. Eggeling, and M. Fritzsche, Nat. Protoc. **12**, 783 (2017).
[28] H. Colin-York, D. Shrestha, J. H. Felce, D. Waithe, E. Moeendarbary, S. J. Davis, C. Eggeling, and M. Fritzsche, Nano Lett. **16**, 2633 (2016).
[29] A. Nicolas, B. Geiger, and S. A. Safran, Proc. Natl. Acad. Sci. U.S.A. **101**, 12520 (2004).
[30] A. Nicolas, A. Besser, and S. A. Safran, Biophys. J. **95**, 527 (2008).
[31] M. Morimatsu, A. H. Mekhdjian, A. S. Adhikari, and A. R. Dunn, Nano. Lett. **13**, 3985 (2013).